# **Yisheng Chen**

Department of Civil Engineering, Zhejiang University, Hangzhou 310058, China

# He Zhang

Department of Hydraulic Engineering, Zhejiang University, Hangzhou 310058, China

# Yangyang Zhang

Department of Civil Engineering, Zhejiang University, Hangzhou 310058, China

# Chunhua Li

Department of Civil Engineering, Zhejiang University, Hangzhou 310058, China

# Qian Yang

Department of Civil Engineering, Zhejiang University, Hangzhou 310058, China

# Hongyu Zheng

Department of Civil Engineering, Zhejiang University, Hangzhou 310058, China

# Chaofeng Lü<sup>1</sup>

Department of Civil Engineering, Zhejiang University, Hangzhou 310058, China; Key Laboratory of Soft Machines and Smart Devices of Zhejiang Province, Zhejiang University, Hangzhou 310027, China; Soft Matter Research Center, Zhejiang University, Hangzhou 310027, China e-mail: luct@zju.edu.cn

# Mechanical Energy Harvesting From Road Pavements Under Vehicular Load Using Embedded Piezoelectric Elements

Highways consume enormous electric power and therefore contribute to heavy economic costs due to the operation of auxiliary road facilities including lighting, displays, and health-monitoring systems for tunnels and bridges, etc. We here propose a new strategy of electric power supply for highways by harvesting mechanical energy from the reciprocating deformation of road pavements. A series of wheel tracking tests are performed to demonstrate the possibility of using piezoelectric elements to transform the mechanical energy stored in pavements due to vehicular load into electricity. An analytical electromechanical model is developed to predict the correlations between electric outputs and loading conditions in the wheel tracking test. A simple scaling law is derived to show that the normalized output power depends on the normalized loading period, location, and size of the piezoelectric device. The scaling law is further extended to a practical highway application according to the analogy between the wheel tracking test and a highway in an idealized condition of periodic vehicular load. It suggests that the output power may be maximized by tuning the material and geometry of the piezoelectric device under various conditions of speed limit and vehicle spacing. The present results may provide a useful guideline for designing mechanical energy-harvesting systems in various road pavements. [DOI: 10.1115/1.4033433]

Keywords: mechanical energy harvesting, wheel tracking test, analytical electromechanical modeling, maximized output electric power, scaling law

> Piezoelectric materials have been widely used for harvesting energy from various ambient energy sources, such as vibrations of

> structures [5-8] or motion of biological organs [9-11], elastic

energy dissipated by absorbers [12], wind or flow water [13],

waste heat [14], electromagnetic waves and solar energy [15], or

those in the occasion with temperature higher than Curie tempera-

ture [16]. Most applications of piezoelectric energy harvesting

from mechanical motions of host structures resort to the match

between resonance frequency of the piezoelectric device and the

excitation frequency so as to attain a maximal energy output

[5–8]. However, this poses a big challenge in practice because of

the high modulus of piezoelectric materials and the associate high

resonance frequency of the energy-harvesting device. In circum-

stances involving low-frequency (1-100 Hz) motions of host

structures, the efficiency of the energy-harvesting devices can

only be optimized through special designing strategies from both the structural and circuit aspects, which includes the modification of materials, geometric configurations, electrode pattern, poling

and stress direction, electric impedance of the circuits, etc. [17].

From this sense, the elastic energy stored in road pavements

due to its reciprocating deformation (frequency  $\sim$ 1 Hz) under ve-

hicular load may also be transformed to electric power using

# 1 Introduction

Highways are always equipped with a large system of lighting, displays for traffic signs or advertisements, and health-monitoring instruments that exhaust a vast amount of electric power every year. In remote area far from urban district, cables for transmitting electric power also contribute to excessive economic costs of considerable amount. Additionally, health-monitoring systems for traffic tunnels and bridges may suffer from malfunction and turnoff once the electric power supply is cut-off due to natural accidents or battery replacement. This will induce breakdown of real-time health monitoring of these transportation infrastructures [1,2]. Harvesting energy from host structures or ambient environment and transforming it into electric power may facilitate to realize long-term self-supply strategies for these highway auxiliary systems [3,4].

Copyright © 2016 by ASME

AUGUST 2016, Vol. 83 / 081001-1

<sup>&</sup>lt;sup>1</sup>Corresponding author.

Contributed by the Applied Mechanics Division of ASME for publication in the JOURNAL OF APPLIED MECHANICS. Manuscript received March 25, 2016; final manuscript received April 16, 2016; published online May 11, 2016. Editor: Yonggang Huang.

piezoelectric energy-harvesting devices. For example, finiteelement modeling was carried out to predict the characteristics of electric outputs of a cymbal piezoelectric energy harvester that is embedded within asphalt mixtures for road pavements [18]. Piezoelectric patches were proposed to integrate with road pavement or railway tracks for energy harvesting, and corresponding infinite Euler–Bernoulli beam models resting on elastic foundations were developed to evaluate the energy-harvesting behavior [19,20]. Jiang et al. [21] designed a roadway energy harvester that contains three multilayer piezoelectric stacks and applied a periodic compression load on the harvester to model the reciprocating vehicular load. They also developed a two degrees-of-freedom electromechanical model to predict the energy conversion efficiency of the energy harvester.

The experiments performed in Refs. [20] and [21] are able to qualitatively reveal the energy-harvesting behavior of piezoelectric elements subject to reciprocating mechanical loading, but they are not adequate to cover the full coupling behavior between road pavement and the energy harvester. We here propose to embed a mechanical energy harvester (MEH) made of lead zirconate titanate (PZT) bimorph within an asphalt track board which is programed with periodic loading through wheel tracking test. In addition, an analytical simple compression model is developed to predict the energy-harvesting behavior of PZT bimorph with excellent agreement with the experimental measurements. A simple scaling law will be derived to show the dependence of the normalized output electric power on the normalized period of rolling wheel, normalized size, and location parameter of the PZT bimorph. This simple scaling law will be further extended to practical highway application using an analogy method by replacing, respectively, the normalized period of rolling wheel and location of PZT bimorph with the normalized vehicle speed and normalized vehicle spacing. The results presented here may serve as a guideline for designing energy harvester in practical road pavement.

#### (size $300 \text{ mm} \times 300 \text{ mm} \times 50 \text{ mm}$ ) is made of hot asphalt mixture, and the embedded MEH device is made of a thickness-polarized PZT bimorph of parallel type which was proved more efficient than the antiparallel bimorph [22]. Each layer of the bimorph (thickness 0.2 mm) has an effective area of $48 \text{ mm} \times 48 \text{ mm}$ to collect electric charge (Figs. 1(*a*) and 1(*b*)). To avoid direct contact between the PZT bimorph and the aggregates of the asphalt mixture, the bimorph is enveloped by two layers of soft rubbers (~2.0 mm thickness). The MEH device is embedded in the asphalt mixture specimen at a depth of ~10 mm, and the test wheel is set to roll along a specific path across the MEH device (Fig. 1(*d*)).

The test wheel (width 50 mm) poses an effective load of 0.8 MPa on the top surface of the specimen (contact length  $\sim$ 20 mm) and rolls across the specimen back-and-forth at a frequency of about 21.64 cycles per min, which gives a period of T = 2.774 s (Fig. 1(c)). The wheel rolls along two different paths (Fig. 2(a)), one along the central axis of the track board specimen (path 1) and the other eccentric to the central axis by 90 mm (path 2). After rolling the wheel for 0.5 min in each individual wheel tracking test, we acquire a steady-state output voltage from an oscilloscope (Figs. 2(b)-2(f)). The phenomenon that the measured output voltage from the device at the center on path 2 (Fig. 2(c)) is higher than that on path 1 (Fig. 2(e)) is mainly due to the decreasing thickness of coverage asphalt from the center toward the edge of the specimen. It should also be mentioned that both Figs. 2(d) and 2(f) are for the same distance (86 mm) along path 1 but these two measurements are taken from independent wheel tracking tests for two specimens. In general, the chronic output voltage exhibits a periodic feature as a response to the corresponding periodic rolling of the wheel. The measurements demonstrate that the MEH device responses to the wheel load only if the wheel becomes overlap with the MEH device, with a peak voltage of  $1.22\pm0.4V$ . Once the wheel passes over the device, the output voltage attenuates until the next overlap occurs.

# 2 Experiments

We designed a wheel tracking test for an asphalt mixture specimen to examine the effectiveness of MEH devices made of piezoelectric materials in asphalt pavement. The track board specimen A theoretical electromechanical model will be developed to evaluate the effectiveness of the MEH device in the wheel rolling test and to investigate the effects of various material and

**3** Theoretical Modeling

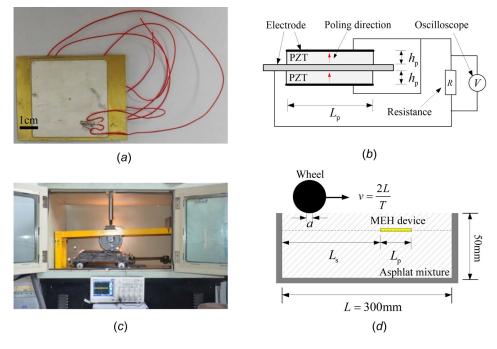


Fig. 1 Schematic illustrations of the MEH and the wheel tracking test setup: (*a*) photograph of the PZT bimorph, (*b*) cross section illustration of the parallel type PZT bimorph with circuit connections, and (*c*) photograph and (*d*) cross section illustration of the wheel tracking test setup with an embedded PZT bimorph

081001-2 / Vol. 83, AUGUST 2016

**Transactions of the ASME** 

geometric factors on the electric outputs. To facilitate simple analytical modeling, the following basic hypotheses are made:

- (1) The mechanical and electrical effects of the MEH device on the mechanical responses of the track board specimen are ignored.
- (2) The dynamic effects of the MEH device are neglected because the frequency of rolling wheel is much lower than the resonance frequency of the PZT bimorph.
- (3) Since little voltage signals were detected when the rolling wheel has no overlap with the MEH device (Figs. 2(b)-2(f)), the MEH device is assumed to be stressed and undergoes mechanical deformation only if the rolling wheel has overlapped with the device.
- (4) The asphalt mixture layer covering the MEH device is much thinner than the total track board specimen, the wheel load attenuates little within the thickness of the cover layer. In addition, the contact length ( $\sim 20 \text{ mm}$ ) between the wheel and the track board is comparable with the MEH

device  $(50 \text{ mm} \times 50 \text{ mm})$ , the PZT bimorph is therefore assumed in a state of simple compression through thickness direction.

According to the above assumptions, the maximal compression stress  $\sigma_{z,max}$  of the bimorph occurs when the wheel overlaps with the device at the center, and it may be defined as

$$\sigma_{z,\max} = -\frac{q_0 a}{L_p} \tag{1}$$

where  $q_0$  is the magnitude of the wheel load, *a* is the contact length of the wheel and the specimen, and  $L_p$  is the length of the PZT bimorph.

The stress evolution in the bimorph, zero-peak-zero, when the wheel rolls through the device, is assumed as a sinusoidal function. Therefore, the entire stress evolution in the bimorph during one period T of rolling wheel may be written as

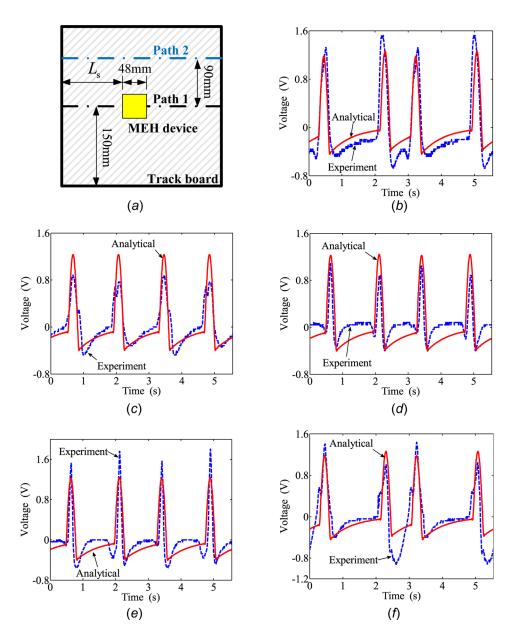


Fig. 2 Comparisons of the real-time output voltage from the experimental measurements and analytical calculations (T = 2.774s): (a) the horizontal illustration of the specimen with the embedded PZT bimorph, (b)  $L_s = 136$  mm for path 2, (c)  $L_s = 126$  mm for path 2, (d)  $L_s = 86$ mm for path 1, (e)  $L_s = 126$  mm for path 1, and (f)  $L_s = 86$  mm for path 1

**Journal of Applied Mechanics** 

AUGUST 2016, Vol. 83 / 081001-3

$$\sigma_{z}(t) = \begin{cases} 0 & 0 \le t \le t_{1} \\ \sigma_{z,\max} \sin\left(\frac{t-t_{1}}{t_{2}-t_{1}}\pi\right) & t_{1} \le t \le t_{2} \\ 0 & t_{2} \le t \le T-t_{2} \\ \sigma_{z,\max} \sin\left(\frac{t+t_{2}-T}{t_{2}-t_{1}}\pi\right) & T-t_{2} \le t \le T-t_{1} \\ 0 & T-t_{1} \le t \le T \end{cases}$$
(2)

where  $t_1 = L_s T/2L$  and  $t_2 = (L_s + L_p + a)T/2L)$ , with  $L_s$  denoting the distance from the specimen edge to the PZT bimorph.

The PZT is transversely isotropic with the three-dimensional constitutive relation, which reads as [23]

$$D = d\sigma + kE \tag{3}$$

where D,  $\sigma$ , and E are, respectively, the column matrices of electric displacement, strain, and electric intensity, and d and k are, respectively, the matrix of piezoelectric constant and dielectric constant at a fixed stress. For the current simple compression model, the thickness-wise electric displacement may be simplified as

$$D_z = d_{33}\sigma_z + k_{33}\frac{V}{h_p} \tag{4}$$

where  $d_{33}$  and  $k_{33}$  are, respectively, the piezoelectric and dielectric constants, while the electric intensity  $E_z = V/h_p$  is implied, with  $h_p$  and V denoting the thickness of and voltage drop across the thickness of each individual PZT layer of the bimorph. The electric charge collected on the electrode of each PZT layer is given by  $Q = D_z b_p L_p$ , where  $b_p$  is the width of the PZT layer. For a closed circuit, the current generated by each individual PZT layer of the bimorph is then defined as I = -dQ/dt. On the other hand, for the parallel connected PZT bimorph, the total output voltage acquired from the oscilloscope equals to that of each PZT layer of the bimorph. Then, the current passing through the oscilloscope is 2I = V/R, where R is the resistance of the oscilloscope. Combining the above electric equilibrium condition and the definition of current gives rise to the differential equation governing the output voltage V from the MEH device as

$$\frac{\mathrm{d}V}{\mathrm{d}t} + \frac{h_{\mathrm{p}}}{2b_{\mathrm{p}}L_{\mathrm{p}}k_{33}R}V = -\frac{d_{33}h_{\mathrm{p}}}{k_{33}}\frac{\mathrm{d}\sigma_{z}}{\mathrm{d}t}$$
(5)

The general solution for Eq. (5) is

$$V(t) = V_0 e^{-\frac{h_{\rm p}t}{2b_{\rm p}L_{\rm p}k_{33}R}} - \frac{d_{33}h_{\rm p}}{k_{33}} \int_0^t \frac{\mathrm{d}\sigma_z}{\mathrm{d}t'} \exp\left[\frac{h_{\rm p}(t'-t)}{2b_{\rm p}L_{\rm p}k_{33}R}\right] \mathrm{d}t' \qquad (6)$$

where  $V_0$  is the initial output voltage at time t = 0. This solution indicates that the output voltage depends on the initial condition which vanishes as  $t \to \infty$ . However, the experimental measurements show that the output voltage always keeps periodic after a few cycles. This is consistent with the fact that, upon a periodic input, the outputs from a first-order differential circuit governed by Eq. (5) are stationary from a long-range view point. That is, the transient part of the solution in Eq. (6) will attenuate rapidly along time with the attenuation velocity depending on the factor  $h_p/(2b_pL_pk_{33}R)$ . In practice, the stationary part of the solution in Eq. (6) is more useful to study the electromechanical responses of the current MEH device.

To derive the stationary solution to Eq. (5), we expand the periodic stress in PZT bimorph  $\sigma_z(t)$  into the following Fourier series:

$$\sigma_z(t) = \frac{\sigma_0}{2} + \sum_{n=1}^{\infty} \sigma_n \cos \frac{n\pi t}{T}$$
(7)

where

$$\sigma_0 = \frac{2}{T} \int_0^T \sigma_z(t) dt = \frac{4\sigma_{z,\max}L_p + a}{\pi L}$$
(8*a*)  
$$\sigma_n = \frac{4\left[1 + (-1)^n\right]}{\pi L_p + a} \frac{\sigma_{z,\max}L}{L_p + a} \left[ \left(\frac{2L}{L_p + a}\right)^2 - n^2 \right]^{-1}$$
(8*b*)

Substituting Eq. (7) into Eq. (5) leads to the stationary solution as

$$V(t) = -\frac{d_{33}h_{\rm p}}{2k_{33}}\sum_{n=1}^{\infty}\sigma_n \left[\cos\frac{n\pi t}{T} + \cos\left(\frac{n\pi t}{T} + 2\varphi_n\right)\right] \tag{9}$$

where  $\varphi_n = \arctan[h_p T/(2n\pi b_p L_p k_{33}R)]$ , indicating that the output voltage has a phase lag relative to the applied mechanical load.

For the current PZT bimorph, the piezoelectric and dielectric constants are, respectively,  $d_{33} = 6.70 \times 10^{-10} \text{ Cm}^{-2}$  and  $k_{33} = 3.01 \times 10^{-8} \text{ Fm}^{-1}$  as provided by the manufacturer, while the electric resistance of the oscilloscope is  $R = 1 \text{ M}\Omega$ . Other parameters involved in the experimental setup are L = 300 mm,  $L_p = b_p = 48 \text{ mm}$ ,  $h_p = 0.2 \text{ mm}$ , a = 20 mm, and  $q_0 = 0.8 \text{ MPa}$ . For different values of  $L_s$  (86 mm, 126 mm, and 136 mm) and rolling paths, the theoretical predictions for the real-time output voltage according to Eq. (9) agree very well with the experimental measurements (Figs. 2(*b*)-2(*f*)).

To evaluate the energy-harvesting behavior of the MEH device, we define the effective voltage as  $V_{\text{RMS}} = \sqrt{T^{-1} \int_0^T V^2 dt}$  (root mean square) and effective output power as  $P = V_{\text{RMS}}^2/R$ . For the experimental setup with  $L_s = 86$  mm, the variations of the effective voltage  $V_{\text{RMS}}$  and output power P versus the electric resistance R and the thickness  $h_p$  of the PZT layer are presented in Fig. 3. The effective voltage increases monotonically and saturates as R approaches infinity which corresponds to the case of open circuit, while the output power attains a maximum for a certain electric resistance (Fig. 3(*a*)). Both electric outputs increases (Fig. 3(*b*)). In addition to the real-time output voltage (Fig. 2), the analytical predictions for the effective voltage and output power ( $L_s = 86$  mm) also agree very well with the experiments (Fig. 3).

Quantitatively, the output power from the bimorph is about  $0.4 \,\mu\text{W}$  (Fig. 3(*b*)), which is a very low power density. However, for road pavement application, we may embed a large number of this type of bimorph along the two wheelpaths. For simple estimation, if we put five bimorph in the wheelpath width direction and spaced 0.15 m along the wheelpath, the output power will reach 200 W if a queue of (e.g., 100) double-axis trunks travel a distance of 100 km. Combining with optimal circuit designs, the harvested energy is applicable for lighting low-power LEDs for road signs or lighting systems.

## 4 Scaling Law

The expressions for the real-time voltage, effective voltage, and effective output power are very complex since they depend on multiple material parameters (e.g., piezoelectric constant  $d_{33}$  and dielectric constant  $k_{33}$ ), geometrical parameters (e.g., length of the specimen *L*, distance of the edges of bimorph and the specimen  $L_s$ , contact length *a*, thickness of the individual piezoelectric layer  $h_p$ , and length and width of the bimorph  $L_p$  and  $b_p$ ), and electric resistance of the oscilloscope *R*. In this section, we will establish a

## Transactions of the ASME

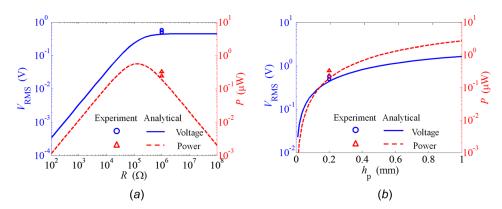


Fig. 3 Variations of the effective output voltage  $V_{\text{RMS}}$  and output power *P* versus (*a*) the electric resistance *R* and (*b*) the thickness  $h_p$  of individual layer of the PZT bimorph

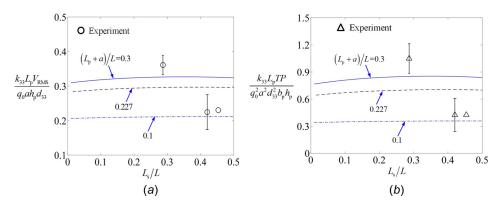


Fig. 4 Variations of (a) the normalized output voltage  $k_{33}L_pV_{RMS}/(q_0ah_pd_{33})$  and (b) normalized output power  $k_{33}L_pTP/(q_0^2a^2d_{33}^2b_ph_p)$  versus the nondimensional distance  $L_s/L$  for various nondimensional effective interaction lengths  $(L_p+a)/L$  with an experimental value  $Th_p/(b_pL_pk_{33}R) = 8.0$ 

simple scaling law for the electric outputs to analyze the intrinsic links between these outputs and various parameters.

By introducing the characteristic voltage  $V_0 = q_0 a h_p d_{33}/(k_{33}L_p)$ and time  $t_0 = b_p L_p k_{33} R/h_p$  and noticing Eq. (8*b*), the nondimensional output voltage in Eq. (9) is derived as

$$\frac{V(\tau)}{V_0} = \frac{1}{\pi} \sum_{m=1}^{\infty} \bar{\sigma}_m \left[ \cos \frac{2m\pi\tau}{\bar{T}} + \cos\left(\frac{2m\pi\tau}{\bar{T}} + 2\arctan\frac{\bar{T}}{4m\pi}\right) \right]$$
(10)

where  $\tau = t/t_0$ ,  $\bar{T} = T/t_0$ , and  $\bar{\sigma}_m = [\cos(\bar{L}_s m\pi) + \cos(\bar{L}_s m\pi + \bar{L}_p m\pi)]/(\bar{L}_p^{-1} - \bar{L}_p m^2)$  is a nondimensional parameter depending on  $\bar{L}_s = L_s/L$  and  $\bar{L}_p = (L_p + a)/L$ . Accordingly, the following normalized effective output voltage and electric power are obtained:

$$\frac{V_{\text{RMS}}}{V_0} = \bar{V}_{\text{RMS}} \left( \frac{T}{t_0}, \frac{L_s}{L}, \frac{L_p + a}{L} \right) \tag{11}$$

$$\frac{P}{P_0} = \bar{P}\left(\frac{T}{t_0}, \frac{L_s}{L}, \frac{L_p + a}{L}\right) \tag{12}$$

where  $P_0 = q_0^2 a^2 d_{33}^2 h_p b_p / (k_{33} L_p T)$  is a characteristic electric power. The above expressions present the scaling laws for the effective voltage and output power, that is, the normalized electric outputs depend only on three nondimensional parameters, i.e., the time scale  $T/t_0$  and the length scales  $L_s/L$ ,  $(L_p + a)/L$ . For a given value of  $T/t_0 = 8$  (experimental setup), the normalized

## Journal of Applied Mechanics

electric outputs change little as  $L_s/L$  varies (Fig. 4) but increase significantly as  $(L_p + a)/L$  increases (Fig. 5). For a given value of  $(L_p + a)/L = 0.227$  (experimental setup), the normalized effective voltage decreases monotonically as  $T/t_0$  increases, while the normalized output power attains a maximum for a certain value of  $T/t_0$  (Fig. 6).

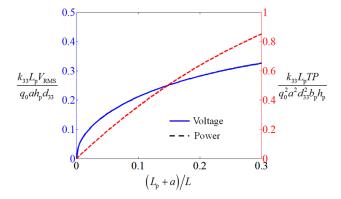


Fig. 5 Variations of the normalized output voltage  $k_{33}L_p V_{RMS}/(q_0 a h_p d_{33})$  and output power  $k_{33}L_p TP/(q_0^2 a^2 d_{33}^2 b_p h_p)$  versus the nondimensional effective interaction length  $(L_p + a)/L$  with experimental values of  $L_s/L = 0.287$  and  $Th_p/(b_p L_p k_{33} R) = 8.0$ 

## AUGUST 2016, Vol. 83 / 081001-5

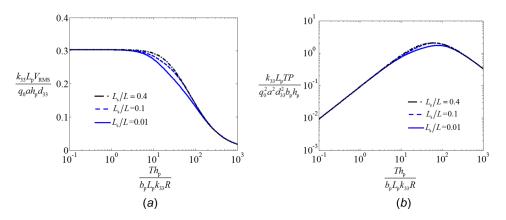


Fig. 6 Dependence of (a) the normalized output voltage  $k_{33}L_p V_{RMS}/(q_0 ah_p d_{33})$  and (b) normalized output power  $k_{33}L_p TP/(q_0^2 a^2 d_{33}^2 b_p h_p)$  on the normalized period  $Th_p/(b_p L_p k_{33}R)$  for various nondimensional distance  $L_s/L$  (( $L_p+a$ )/L=0.227)

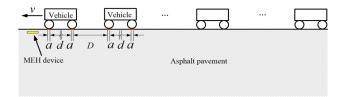


Fig. 7 The practical road pavement with one MEH device and subject to a queue of periodic vehicles traveling at a same speed v which is analogous to the wheel tracking test in Fig. 1(*d*)

#### 5 Engineering Application

The present experimental setup and theoretical modeling may be extended to applications for piezoelectric energy harvesting in practical road pavement. To this end, the back-and-forth rolling of the wheel and across the MEH device in the current experiment is analogous to a queue of equal-spacing vehicles traveling at a constant speed and across one MEH device (Fig. 7). In general, the rolling distance  $2L_s$  may be analogous to the vehicle spacing D, which here is defined as the distance between the back axle of the front vehicle and the front axle of the back vehicle, while  $2(L - L_p - a - L_s)$  analogous to the wheelbase d of an individual vehicle.

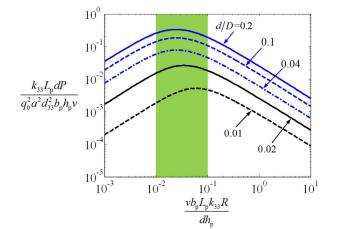
Based on the above analogy, we may replace the parameters L and  $L_s$  in the current wheel tracking test by the traffic parameters

*D* and *d* according to the relations  $L_s = D/2$  and  $L = (D + d/2) + L_p + a$ . Substituting them into Eq. (12), the scaling law for piezoelectric energy harvesting from practical asphalt pavement may be expressed as

$$\frac{P}{\tilde{P}_0} = \tilde{P}\left(\frac{v}{v_0}, \frac{d}{D}, \frac{L_p + a}{d}\right)$$
(13)

where  $\bar{P}_0 = q_0^2 a^2 d_{33}^2 h_p b_p v/(k_{33}L_p d)$  is a power scale, while v is the vehicle speed and  $v_0 = dh_p/(b_p L_p k_{33} R)$  may be termed as the characteristic speed. The function  $\tilde{P}$  is straightforward from Eq. (12) and not presented here for brevity. To ensure the effectiveness of the above model for practical traffic, the ratio  $L_p/a$  is kept the same as the current wheel tracking test. For real vehicles, the contact length between the tire and pavement is at the order of 10 cm, and the wheelbase d differs from one type of vehicle to another. In the following, we consider an ideal situation that the queue of vehicles are intermediate cars whose wheelbase is typically  $2.6 \sim 2.8$  m. With the above conditions, the nondimensional parameter  $(L_p + a)/d$  for all the calculations hereafter is taken as 0.17.

Figure 8 presents the variation of the normalized output power  $P/\tilde{P}_0 = k_{33}L_p dP/(q_0^2 a^2 d_{33}^2 b_p h_p v)$  versus the normalized vehicle speed  $v/v_0 = v b_p L_p k_{33} R/(dh_p)$  for various values of d/D. There exists an optimal electric resistance for attaining a maximal output power as  $v/v_0$  increases. In practice, however, the vehicle speed v is random and kept below the speed limit for any specific road way. That is, for a piezoelectric MEH device with given material



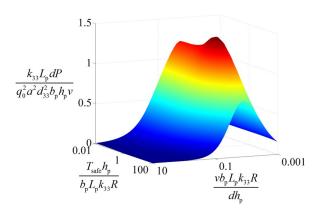
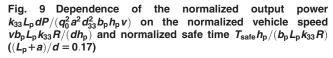


Fig. 8 Dependence of the normalized output power  $k_{33}L_p dP/(q_0^2 a^2 d_{33}^2 b_p h_p v)$  on the normalized vehicle speed  $vb_p L_p k_{33} R/(dh_p)$  for various vehicle spacing d/D (( $L_p + a)/d = 0.17$ )

081001-6 / Vol. 83, AUGUST 2016



Transactions of the ASME

(fixed  $d_{33}$  and  $k_{33}$ ) and geometry (fixed  $L_p$ ,  $b_p$ , and  $h_p$ ), we can only tune the electric resistance to obtain an output power as high as possible. For example, given the current PZT MEH device and vehicle spacing d/D = 0.01, a vehicle speed of 100 km/hr yields a nondimensional output power of about  $10^{-4}$  for  $R = 10^6 \Omega$ , but this power will exceed  $2 \times 10^{-3}$  if the electric resistance decreases to  $R = 10^4 \Omega$ .

Figure 8 also suggests the increasing behavior of output power by decreasing the vehicle spacing *D*. Here, d/D = 0.01 corresponds to traffic flow at the speed limit on express way while d/D = 0.2 denotes the case of low-traveling speed in urban road. The curves in the shadow zone indicate that, for most possible vehicle spacing, we may attain almost the highest output power as long as the energy-harvesting system is designed such that  $0.01 \le v b_p L_p k_{33} R/(dh_p) \le 0.1$ .

In practical traffic, the vehicle spacing always requires a minimal value  $D_{\min}$  for any specific vehicle speed so as to guarantee the traffic safety. In addition, this minimal vehicle spacing  $D_{\min}$ also varies with environmental condition (e.g., rain, snow, or fog). A feasible way for characterizing this minimal vehicle spacing  $D_{\min}$  is to use the so-called safe time,  $T_{\text{safe}}$ , that is needed for a vehicle to travel a distance of  $D_{\min}$  at a certain speed v, i.e.,  $D_{\min} = T_{\text{safe}}v$ . Consider the ideal case that the whole queue of vehicles is spaced by  $D_{\min}$ , the scaling law in Eq. (13) for energy harvesting is further translated to

$$\frac{P}{\tilde{P}_0} = \tilde{P}\left(\frac{v}{v_0}, \frac{T_{\text{safe}}}{t_0}, \frac{L_p + a}{d}\right)$$
(14)

Figure 9 exhibits the surface diagram for the relationship between three normalized quantities, i.e., output power  $P/\tilde{P}_0$ , vehicle speed  $v/v_0$ , and safe time  $T_{\text{safe}}/t_0$ , for  $(L_p + a)/d = 0.17$ . The nondimensional output power  $P/\tilde{P}_0$  attains a peak value when both  $v/v_0$  and  $T_{\text{safe}}/t_0$  increase. For any specific  $T_{\text{safe}}/t_0$ , the nonlinear variation of  $P/\tilde{P}_0$  versus  $v/v_0$  is highly distinguishable with indication of significant effects posed by  $v/v_0$ . In comparison, the effects of the safe time  $T_{\text{safe}}/t_0$  are only obvious when  $v/v_0$  is close to the extreme point for maximal  $P/\tilde{P}_0$  and become increasingly unnoticeable when  $v/v_0$  departs from the extreme point.

#### 6 Conclusion

We have proposed a wheel tracking test to examine the effectiveness of using embedded piezoelectric elements to harvest mechanical energy from asphalt pavement and developed a simple compression model to evaluate the efficiency of the piezoelectric energy harvester. Theoretical calculations exhibited excellent agreement with experiment. A scaling law was derived to show that the normalized output power depends on the normalized period of rolling wheel load, location, and size of the piezoelectric energy harvester. For the purpose of road engineering application, this scaling law was further translated to the case of energy harvesting in a practical road pavement by introducing the normalized vehicle speed and normalized vehicle spacing or safe time. It suggests that the output power of the energy harvester may be optimized by properly selecting material and geometry parameters for practical traffic conditions, i.e., given vehicle speed and vehicle spacing. The results here may provide valuable references for the design of piezoelectric energy harvesting in practical road pavements. Finally, as perspectives, further experiments and theoretical models will be proposed to evaluate the effects embedded depth and the electrical resistive load on the characteristics of the energy harvester.

#### Acknowledgment

The authors acknowledge the funding supports from the National Natural Science Foundation of China (Nos. 11322216, 11321202, and 11472244) and the Zhejiang Provincial Natural Science Foundation of China (No. LR13A020001). It was also partly supported by the Fundamental Research Funds for the Central Universities (No. 2016XZZX001-05).

## References

- Wardlaw, J. L., Karaman, I. K., and Aydin, I., 2013, "Low-Power Circuits and Energy Harvesting for Structural Health Monitoring of Bridges," IEEE Sens. J., 13(2), pp. 709–722.
- [2] McCullagh, J. J., Galchev, T., Peterson, R. L., Gordenker, R., Zhang, Y., Lynch, J., and Najafi, K., 2014, "Long-Term Testing of a Vibration Harvesting System for the Structural Health Monitoring of Bridges," Sens. Actuators A, 217, pp. 139–150.
- [3] Bowen, C. R., Kim, H. A., Weaver, P. M., and Dunn, S., 2014, "Piezoelectric and Ferroelectric Materials and Structures for Energy Harvesting Applications," Energy Environ. Sci., 7(1), pp. 25–44.
- [4] Liu, Z. J., Cheng, H. Y., and Wu, J., 2014, "Mechanics of Solar Module on Structured Substrates," ASME J. Appl. Mech., 81(6), p. 064502.
  [5] Kim, H. S., Kim, J. H., and Kim, J., 2011, "A Review of Piezoelectric Energy
- [5] Kim, H. S., Kim, J. H., and Kim, J., 2011, "A Review of Piezoelectric Energy Harvesting Based on Vibration," Int. J. Precis Eng. Manuf., 12(6), pp. 1129–1141.
- [6] Wu, Z., Harne, R. L., and Wang, K. W., 2014, "Energy Harvester Synthesis Via Coupled Linear-Bistable System With Multistable Dynamics," ASME J. Appl. Mech., 81(6), p. 061005.
- [7] Chen, L., and Jiang, W., 2015, "Internal Resonance Energy Harvesting," ASME J. Appl. Mech., 82(3), p. 031004.
- [8] Boisseau, S., Despesse, G., and Seddik, B. A., 2013, "Nonlinear H-Shaped Springs to Improve Efficiency of Vibration Energy Harvesters," ASME J. Appl. Mech., 80(6), p. 061013.
- [9] Dagdeviren, C., Yang, B. D., Su, Y., Tran, P. L., Joe, P., Anderson, E., Xia, J., Doraiswamy, V., Dehdashti, B., Feng, X., Lu, B., Poston, R., Khalpey, Z., Ghaffari, R., Huang, Y., Slepian, M. J., and Rogers, J. A., 2014, "Conformal Piezoelectric Energy Harvesting and Storage From Motions of the Heart, Lung, and Diaphragm," Proc. Natl. Acad. Sci. U.S.A., 111(5), pp.1927–1932.
- [10] Lu, B., Chen, Y., Ou, D., Chen, H., Diao, L., Zhang, W., Zheng, J., Ma, W., Sun, L., and Feng, X., 2015, "Ultra-Flexible Piezoelectric Devices Integrated With Heart to Harvest the Biomechanical Energy," Sci. Rep., 5, p. 16065.
  [11] Zhang, Y. Y., Chen, Y. S., Lu, B. W., Lu, C. F., and Feng, X., 2016,
- [11] Zhang, Y. Y., Chen, Y. S., Lu, B. W., Lu, C. F., and Feng, X., 2016, "Electromechanical Modeling of Energy Harvesting From the Motion of Left Ventricle in Closed Chest Environment," ASME J. Appl. Mech., 83(6), p. 061007.
- [12] Ali, S. F., and Adhikari, S., 2013, "Energy Harvesting Dynamic Vibration Absorbers," ASME J. Appl. Mech., 80(4), p. 041004.
- [13] McCarthy, J. M., Watkins, S., Deivasigamani, A., and John, S. J., 2016, "Fluttering Energy Harvesters in the Wind: A Review," J. Sound Vib., 361, pp. 355–377.
- [14] Namli, O. C., and Taya, M., 2011, "Design of Piezo-SMA Composite for Thermal Energy Harvester Under Fluctuating Temperature," ASME J. Appl. Mech., 78(3), p. 031001.
- [15] Anton, S. R., and Sodano, H. A., 2007, "A Review of Power Harvesting Using Piezoelectric Materials (2003–2006)," Smart Mater. Struct., 16(3), pp. R1–R21.
- [16] Krichen, S., and Sharma, P., 2016, "Flexoelectricity: A Perspective on an Unusual Electromechanical Coupling," ASME J. Appl. Mech., 83(3), p. 030801.
- [17] Li, H. D., Tian, C., and Deng, Z. D., 2014, "Energy Harvesting From Low Frequency Applications Using Piezoelectric Materials," Appl. Phys. Rev., 1(4), p. 041301.
- [18] Zhao, H. D., Ling, J. M., and Yu, J., 2012, "A Comparative Analysis of Piezoelectric Transducers for Harvesting Energy From Asphalt Pavement," J. Ceram. Soc. Jpn., **120**(1404), pp. 317–323.
- [19] Xiang, H. J., Wang, J. J., Shi, Z. F., and Zhang, Z. W., 2013, "Theoretical Analysis of Piezoelectric Energy Harvesting From Traffic Induced Deformation of Pavements," Smart Mater. Struct., 22(9), p. 095024.
- [20] Wang, J. J., Shi, Z. F., Xiang, H. J., and Song, G. B., 2015, "Modeling on Energy Harvesting From a Railway System Using Piezoelectric Transducers," Smart Mater. Struct., 24(10), p. 105017.
- [21] Jiang, X. Z., Li, Y. C., Li, J. C., Wang, J., and Yao, J., 2014, "Piezoelectric Energy Harvesting From Traffic-Induced Pavement Vibrations," J. Renewable Sustainable Energy, 6(4), p. 043110.
  [22] Lim, C. W., He, L. H., and Soh, A. K., 2001, "Three-Dimensional Electrome-
- [22] Lim, C. W., He, L. H., and Soh, A. K., 2001, "Three-Dimensional Electromechanical Responses of a Parallel Piezoelectric Bimorph," Int. J. Solids Struct., 38(16), pp. 2833–2849.
- [23] Ding, H. J., and Chen, W. Q., 2001, *Three Dimensional Problems of Piezoelasticity*, Nova Science Publishers, New York.

## **Journal of Applied Mechanics**